VEGF Blockade Enables Oncolytic Cancer Virotherapy in Part by Modulating Intratumoral Myeloid Cells

Mark A Currier[1,2], Francis K Eshun[1,3], Allyson Sholl[4], Artur Chernoguz[5], Kelly Crawford[5], Senad Divanovic[4], Louis Boon[6], William F Goins[7], Jason S Frischer[5], Margaret H Collins[8], Jennifer L Leddon[1,2], William H Baird[1], Amy Haseley[9], Keri A Streby[10], Pin-Yi Wang[1,2], Brett W Hendrickson[11], Rolf A Brekken[12], Balveen Kaur[9], David Hildeman[4] and Timothy P Cripe[1,2,10]

[1]Divison of Oncology, Department of Pediatrics, Cincinnati Children's Hospital Medical Center, Cincinnati, Ohio, USA; [2]Center for Childhood Cancer and Blood Diseases, Nationwide Children's Hospital, The Ohio State University, Columbus, Ohio, USA; [3]Division of Hematology/Oncology, Department of Pediatrics, Phoenix Children's Hospital, Phoenix, Arizona, USA; [4]Division of Cellular and Molecular Immunobiology, Department of Pediatrics, Cincinnati Children's Hospital Medical Center, Cincinnati, Ohio, USA; [5]Department of Surgery, Cincinnati Children's Hospital Medical Center, Cincinnati, Ohio, USA; [6]Bioceros B.V., Utrecht, The Netherlands; [7]Department of Microbiology and Molecular Genetics, University of Pittsburgh School of Medicine, Pittsburgh, Pennsylvania, USA; [8]Division of Pathology, Department of Pediatrics, Cincinnati Children's Hospital Medical Center, Cincinnati, Ohio, USA; [9]Department of Neurological Surgery, The Ohio State University, Columbus, Ohio, USA; [10]Division of Hematology/Oncology/BMT, Department of Pediatrics, Nationwide Children's Hospital, The Ohio State University, Columbus, Ohio, USA; [11]Department of Anatomic Pathology and Laboratory Medicine, Nationwide Children's Hospital, The Ohio State University, Columbus, Ohio, USA; [12]Division of Surgical Oncology, Department of Surgery, Hamon Center for Therapeutic Oncology Research, University of Texas Southwestern Medical Center, Dallas, Texas, USA

Understanding the host response to oncolytic viruses is important to maximize their antitumor efficacy. Despite robust cytotoxicity and high virus production of an oncolytic herpes simplex virus (oHSV) in cultured human sarcoma cells, intratumoral (ITu) virus injection resulted in only mild antitumor effects in some xenograft models, prompting us to characterize the host inflammatory response. Virotherapy induced an acute neutrophilic infiltrate, a relative decrease of ITu macrophages, and a myeloid cell-dependent upregulation of host-derived vascular endothelial growth factor (VEGF). Anti-VEGF antibodies, bevacizumab and r84, the latter of which binds VEGF and selectively inhibits binding to VEGF receptor-2 (VEGFR2) but not VEGFR1, enhanced the antitumor effects of virotherapy, in part due to decreased angiogenesis but not increased virus production. Neither antibody affected neutrophilic infiltration but both partially mitigated virus-induced depletion of macrophages. Enhancement of virotherapy-mediated antitumor effects by anti-VEGF antibodies could largely be recapitulated by systemic depletion of CD11b$^+$ cells. These data suggest the combined effect of oHSV virotherapy and anti-VEGF antibodies is in part due to modulation of a host inflammatory reaction to virus. Our data provide strong preclinical support for combined oHSV and anti-VEGF antibody therapy and suggest that understanding and counteracting the innate host response may help enable the full antitumor potential of oncolytic virotherapy.

Received 19 May 2012; accepted 7 February 2013; advance online publication 12 March 2013. doi:10.1038/mt.2013.39

INTRODUCTION

Oncolytic viruses are being developed as anticancer agents. Herpes simplex virus (HSV) is an attractive vector because it can infect a wide variety of different tissues and also has a large genome that can accommodate therapeutic transgenes.[1] A number of different oncolytic HSV (oHSV) mutants have been used in clinical trials in early dose-escalation safety studies and have not revealed any serious adverse effects.[2] Reports of antitumor efficacy have not matched preclinical results, however, raising the possibility of immunologic barriers to efficacy.

Although little is known about the host inflammatory response to oHSV virotherapy in the tumor microenvironment, a number of studies have investigated HSV-1 pathogenesis in other disease models such as herpetic stromal keratitis. HSV-1 infection of corneal epithelial cells induces significant neoangiogenesis and inflammation mediated by a variety of factors including vascular endothelial growth factor (VEGF-A).[3–8] These inflammatory signals in response to HSV-1 infection are similar to the proinflammatory and cell-recruitment signals in tumors, mediated in part by tumor cells as well as macrophages in the tumor microenvironment. Tumor-associated macrophages (TAMs) play profound and diverse roles in tumors through both direct contacts and paracrine effects that impact/regulate tumorigenesis, vasculogenesis, tumor cell growth, extracellular matrix deposition/remodeling, and response to therapy, and in general are either tumoricidal (M1-type) or protumorigenic (M2-type) (see reviews, refs. 9–11).

Multiple antiangiogenic therapies are Food and Drug Administration-approved for cancer such as anti-VEGF–A antibody (bevacizumab) and various inhibitors of VEGF receptor (VEGFR) signaling. Interestingly, recent studies have shown that VEGF blockade not only reduces VEGF-mediated angiogenesis,

Correspondence: Timothy P Cripe, Division of Hematology/Oncology/BMT, Nationwide Children's Hospital, 700 Children's Drive, Columbus, Ohio 43205, USA. E-mail: timothy.cripe@nationwidechildrens.org

but also modulates intratumoral (ITu) cytokine expression such as interleukin-1β, interleukin-6, and CXCL1 and significantly reduces recruitment of immunosuppressive cells such as macrophages, regulatory T cells, and myeloid-derived suppressor cells.[12] These effects appear mediated by VEGF-A binding to VEGFR2, as determined using the antibody r84 that binds VEGF-A and selectively blocks its interaction with VEGFR2 without interfering with binding to VEGFR1.[13,14]

In this study, we sought to determine whether a proangiogenic response occurs during oHSV virotherapy for cancer, to what extent it may limit antitumor efficacy, and if it could be counteracted by antiangiogenic therapy. We previously noted that oHSVs exhibit variable antitumor efficacy even in cases where cultured cells are highly susceptible to virus infection. Here, we primarily studied a sarcoma model highly susceptible in tissue culture to virus infection but which exhibited very little tumor response *in vivo*. The use of a xenograft model enabled us to distinguish tumor-derived (human) from host-derived (mouse) VEGF-A (heretofore referred to as VEGF). Our studies provide compelling evidence that oHSV infection induces a marked ITu inflammatory cellular response characterized by neutrophilic infiltration and a decrease of ITu macrophages. Furthermore, we found that anti-VEGF antibodies enhance the antitumor effect of virotherapy. The mechanism was not only *via* an antiangiogenic effect but also by modulating the composition of ITu myeloid cells, as the effect of combination therapy could be recapitulated by myeloid cell depletion before virotherapy.

RESULTS

Human sarcoma xenografts exhibit variable response to oHSV despite robust virus effects in cell culture

The ICP-6 mutant oncolytic virus rRp450 showed robust virus production of 3–4 logs in a panel of sarcoma cell lines (**Figure 1a**). Replication correlated with cytotoxicity, as shown for A673 cells with no viable cells remaining by day 3 post-infection at even the lowest multiplicities of infection (MOI) tested (**Figure 1b**). Mice bearing Ewing sarcoma A673 or osteosarcoma 143.98.2 xenografts were treated with two doses of ITu rRp450 or phosphate-buffered

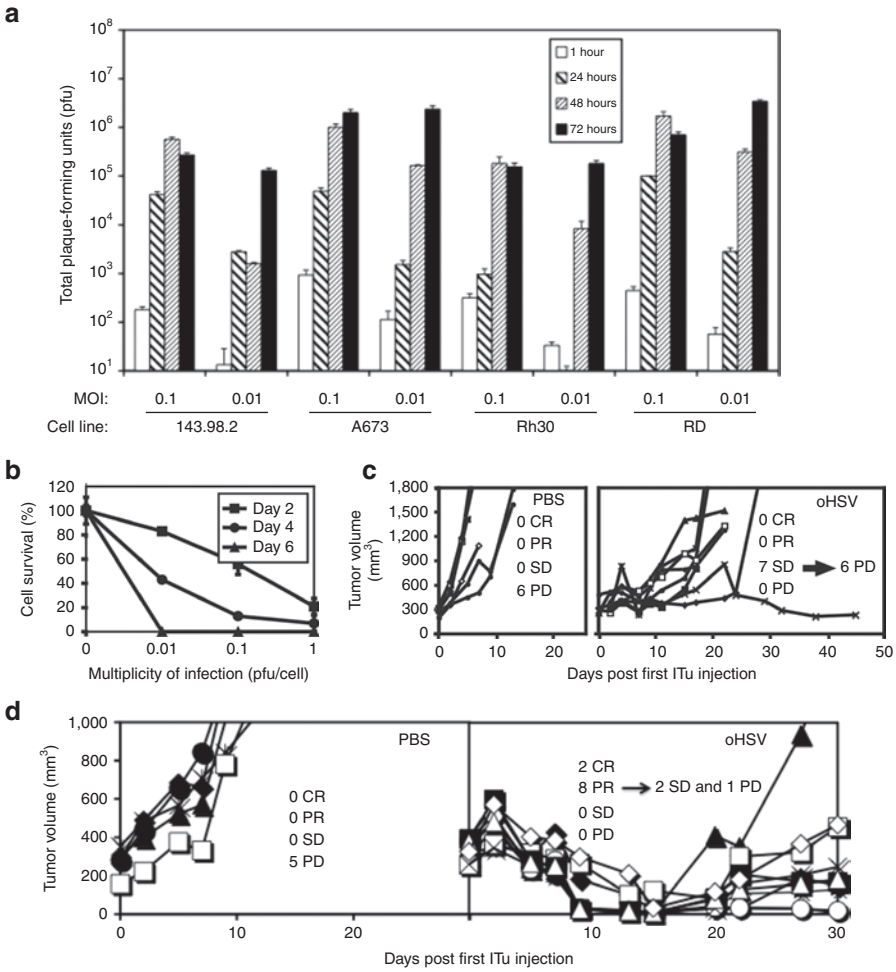

Figure 1 Analysis of rRp450 efficacy in sarcoma models. (**a**) Tumor cells were infected with rRp450 at the indicated MOI and harvested for HSV titer as determined by standard plaque assay at 1, 24, 48, and 72 hours post-infection ($n = 4$). Error bars represent SEM. (**b**) A673 cells were infected at the indicated MOI and cell viability was measured on days 2, 4, and 6 by MTT assay ($n = 4$). Error bars represent SD. (**c**) Mice bearing A673 tumors received two intratumoral injections of rRp450 at 1×10^7 pfu or PBS control, on days 0 and 2, and then followed for tumor growth ($n = 7$). (**d**) Mice bearing 143.98.2 tumors received two intratumoral injections of rRp450 at 1×10^7 pfu or PBS as a control on days 0 and 2, and were followed for tumor growth ($n = 5$–10). CR, complete response; ITu, intratumoral; MOI, multiplicity of infection; oHSV, oncolytic herpes simplex virus; PBS, phosphate-buffered saline; pfu, plaque-forming unit; PD, progressive disease; PR, partial response; SD, stable disease.

saline (PBS, control) and followed for survival. In the A673 model, all of the control mice showed tumor progression and required euthanization by day 13, whereas oHSV (rRp450)-treated mice showed slowing of tumor growth, albeit only to a moderate degree (seven of seven stable disease (SD)) and ultimately progressed, except one animal that exhibited long-term SD (**Figure 1c**). Interestingly, all of the virus-treated mice bearing 143.98.2 tumors responded with significant tumor shrinkage (2/10 complete responses and 8 partial responses, though by day 30 one tumor progressed (progressive disease, **Figure 1d**)). These data revealed a disconnect between tumor cell autonomous susceptibility to oHSV infection and *in vivo* antitumor effects in the A673 model. Given the absence of T cells in the animals, these data raised the possibility of an innate inflammatory response to virus infection that might be limiting the antitumor efficacy of virotherapy.

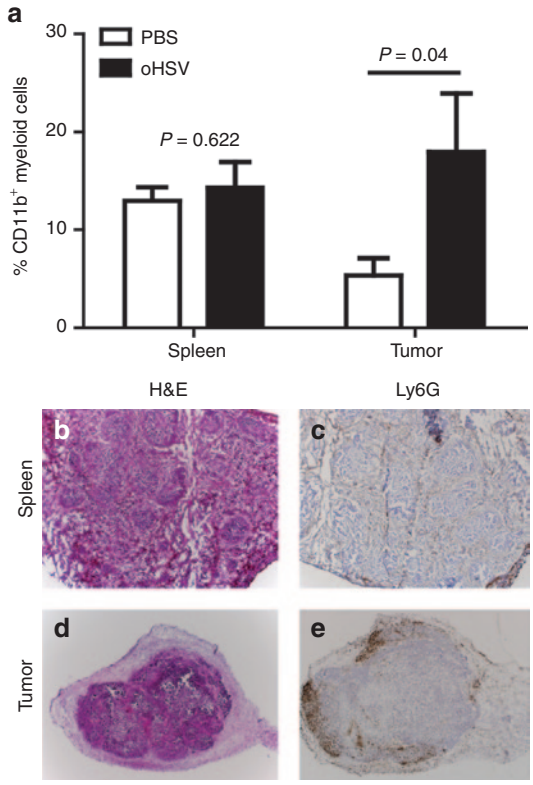

Figure 2 Recruitment of myeloid cells in oHSV-injected tumors. A673 xenograft tumors were injected with rRp450 or PBS control. (**a**) The relative numbers of CD11b$^+$ myeloid cells in the spleen (n = 4–5, t-test) and infected flank tumors (n = 6, t-test) were determined 3 days after virus injection by flow cytometry. In a separate experiment, (**b**,**c**) spleens and (**d**,**e**) tumors were collected 24 hours after virus injection and analyzed by hematoxylin and eosin (H&E) and by Ly6G immunohistochemistry staining (4X objective). The spleen served as a control, and brown staining is restricted to the red pulp and absent from the white pulp. oHSV, oncolytic herpes simplex virus; PBS, phosphate-buffered saline.

oHSV infection recruits CD11b$^+$ myeloid cells and induces stroma-derived VEGF production in A673 xenograft tumors

During native HSV infection, the host inflammatory response results in myeloid cell infiltration and local production of proangiogenic factors such as VEGF.[7] We sought to determine whether oHSV injection causes a similar cellular infiltrate in the tumor microenvironment. ITu oHSV increased the presence of CD11b$^+$ cells in A673 tumors by fourfold, with no change of cell numbers in the spleen (**Figure 2a**). Consistent with these data, we stained virus-infected tumors for neutrophils using an anti-Ly6G antibody and saw a robust infiltration as early as 24 hours post-infection (**Figure 2b–e**). Interestingly, the infiltration was predominantly along the tumor periphery, though neutrophils were scattered throughout the tumor as well. ITu human VEGF (hVEGF) levels decreased by 3.4-fold following oHSV injection (**Figure 3a**, $P < 0.0001$), presumably due to tumor cell destruction. Mouse VEGF (mVEGF) levels increased by 3.6-fold in virus-treated mice compared with controls (**Figure 3b**). A caveat of these experiments is that we do not know the relative numbers of tumor or stromal cells in the tumors and we have thus normalized the levels to total protein; because the tumors may differ in their composition of stroma including fibrosis and necrosis, we cannot ascertain the data reflecting changes in expression on a per cell basis. Nevertheless, these findings suggest that virus treatment elicited an innate host response involving myeloid cells and proangiogenic chemokines.

Myeloid cells are responsible for virus-induced stroma-derived VEGF

Our observation that virus-induced, host-derived mVEGF corresponded with a myeloid cellular infiltration suggested that

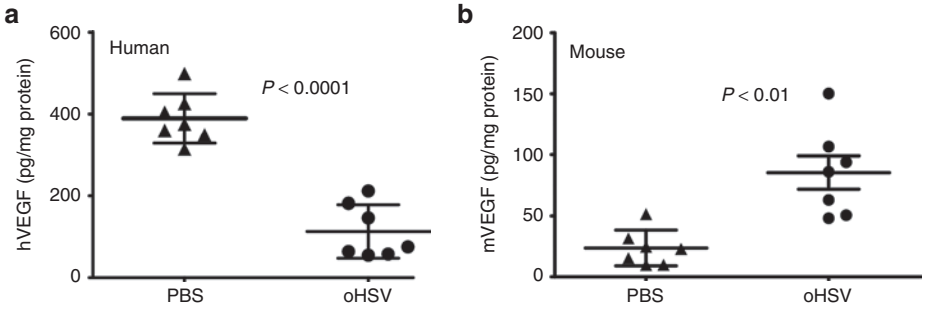

Figure 3 Induction of mVEGF in oHSV-injected tumors. A673 xenograft tumors were injected with rRp450 or PBS control and tumors were harvested at 3 days. The amount of (**a**) tumor-derived hVEGF (n = 7) and (**b**) stroma-derived mVEGF was determined by ELISA (n = 7). Error bars represent SEM. ELISA, enzyme-linked immunosorbent assay; hVEGF, human vascular endothelial growth factor; mVEGF, mouse vascular endothelial growth factor; oHSV, oncolytic herpes simplex virus; PBS, phosphate-buffered saline.

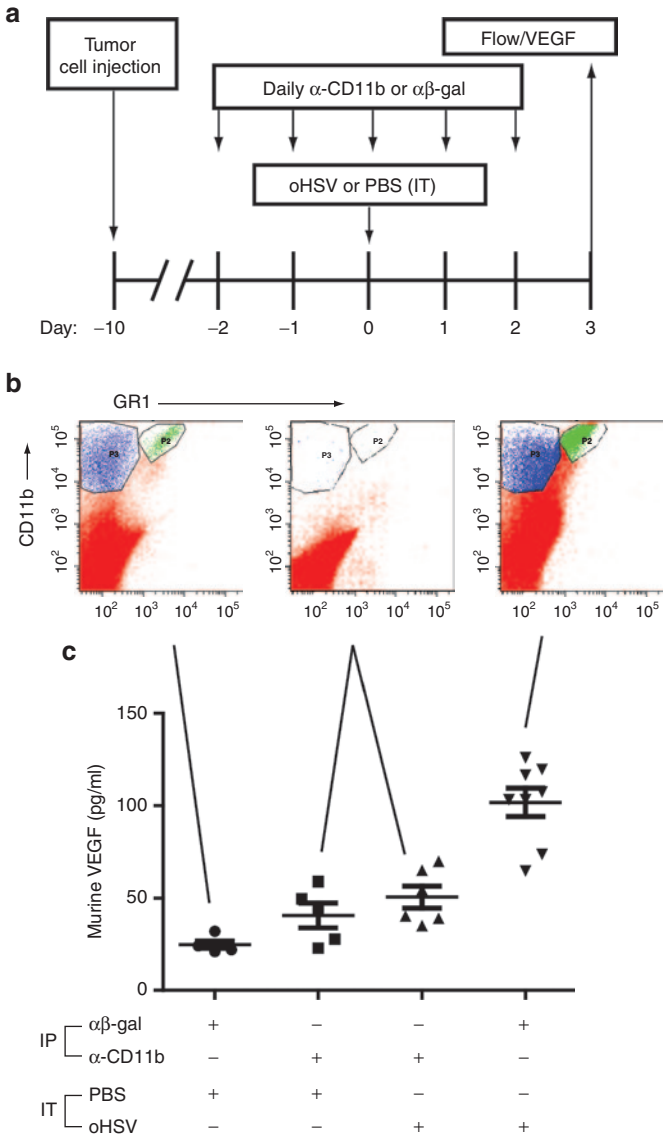

Figure 4 Depletion of CD11b$^+$ cells in oHSV-injected tumors. (**a**) A673 tumor-bearing animals were administered intraperitoneally either αβ-gal antibody (control) or α-CD11b antibody on the indicated days and either intratumoral PBS (control) or rRp450 (oHSV) on day 0. (**b**) Tumors were collected at day +3 and analyzed by flow cytometry. Shown are representative scatter plots from an $n = 3$ experiment illustrating the baseline CD11b$^+$ and GR1$^+$ populations, their depletion by anti-CD11b antibody injection, and their increase with oHSV infection. Only one scatter plot is shown for CD11b depletions because all six were essentially identical, with absence of CD11b cells regardless of PBS or oHSV injection. (**c**) Tumors were analyzed by ELISA for murine VEGF production ($n = 5$–8). Error bars represent SEM. ELISA, enzyme-linked immunosorbent assay; IP, intraperitoneal; IT, intratumoral; oHSV, oncolytic herpes simplex virus; PBS, phosphate-buffered saline; VEGF, vascular endothelial growth factor.

these cells may be responsible for increased production of mVEGF, similar to models of HSV-1–induced keratitis.[12] We used a systemic cellular depletion strategy (Figure 4a) to test this hypothesis. Intraperitoneal (IP) anti-CD11b antibody effectively depleted ITu CD11b$^+$ cells (Figure 4b) and prevented the virus-induced increase in stroma-derived mVEGF (Figure 4c). These findings suggest that CD11b$^+$ myeloid cells are responsible either directly or indirectly for increased mVEGF following oHSV injection.

VEGF blockade enhances the antitumor efficacy of oHSV

Although the ITu hVEGF and thus total VEGF (hVEGF + mVEGF) decreased following oHSV, the increase in mVEGF suggested that VEGF blockade may enhance antitumor efficacy of virotherapy. We thus followed A673 tumor growth in animals bearing large tumors (mostly 500–1,000 mm^3) given ITu oHSV in combination with the anti-hVEGF antibody bevacizumab or the anti-h/mVEGF r84. Although bevacizumab is human specific (data not shown), r84 binds both hVEGF and mVEGF.[14] Because of its different binding epitope, r84 selectively blocks VEGF binding to VEGFR2 but allows binding to VEGFR1 to remain intact.[14] All mice given ITu saline and IP control antibody showed tumor progression and required euthanization by day 17 (**Supplementary Figure S1a**). Mice given ITu oHSV showed minimal slowing of tumor growth with six of seven animals experiencing progressive disease requiring euthanization by day 24 and only one with SD that ultimately progressed (**Supplementary Figure S1b**). Animals treated with bevacizumab alone demonstrated a more durable response with two of seven animals exhibiting a complete response; however, five of seven progressed (**Supplementary Figure S1c**). Animals given the combination of bevacizumab and oHSV showed a response rate of 75% (six of eight) with four SDs beyond 30 days, one partial response that remained a SD at day 60, one complete response, and two progressive diseases (**Supplementary Figure S1d**). Interestingly, all animals treated with saline and r84 showed tumor progression and required euthanization by day 14 (**Supplementary Figure S1e**). Previous studies showed prevention of tumorigenesis of A673 by a r84-like antibody, but effects on established tumors were not tested.[15] In contrast, animals given oHSV and r84 showed a number of durable responses with 57% (four of seven) having SD that lasted beyond 30 days (**Supplementary Figure S1f**). Three of these animals eventually progressed.

The antitumor effects of combination therapy were even more dramatic in a repeat experiment with bevacizumab using somewhat smaller tumors (200–350 mm^3). As before, control mice progressed rapidly and had to be killed within 10 days (Figure 5a). Median survival was prolonged to 18.5 and 28 days for bevacizumab-treated and oHSV-treated mice, respectively (Figure 5b). Statistically, there was no difference in survival between bevacizumab-treated mice and oHSV-treated mice ($P = 0.44$). Median survival was markedly increased by combination therapy, with survival of 85% when the experiment was terminated at 60 days.

Altogether, our findings suggest that VEGF blockade enhances the antitumor efficacy of oHSV virotherapy. Notably, the effect was similar for both anti-VEGF antibodies, even though bevacizumab has no effect on mVEGF, suggesting that the tumor-derived hVEGF remains predominant following virotherapy in this tumor model.

Bevacizumab represses oHSV replication in A673 tumors

We next measured the effect of bevacizumab on ITu virus replication to determine whether the improved antitumor efficacy of

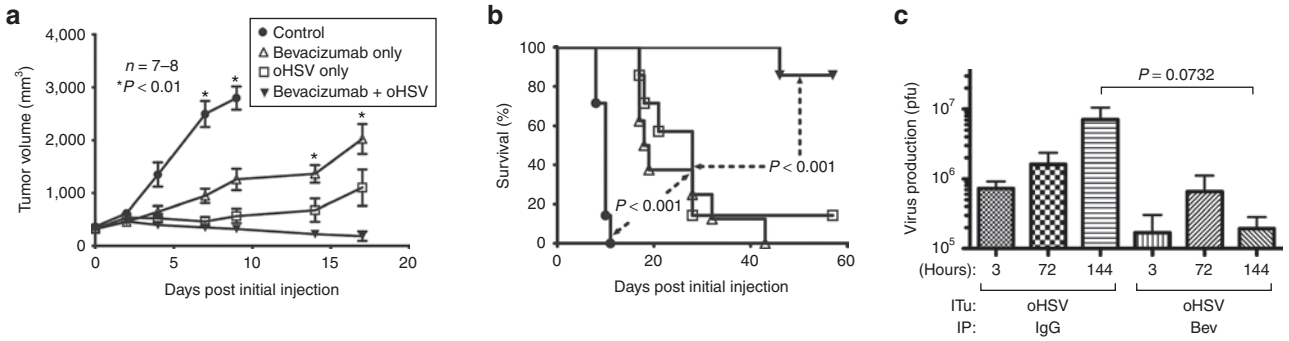

Figure 5 Treatment of A673 xenografts with combination bevacizumab and oHSV. Mice bearing A673 xenografts were treated with ITu oHSV, IP bevacizumab or a combination of both and followed for (**a**) tumor growth (n = 7–8) and (**b**) survival (n = 7–8). Error bars represent SEM. (**c**) Intratumoral virus production was measured in a separate cohort. Tumors were harvested at times shown and measured for infectious virus particles by plaque assay. Bevacizumab reduced virus production in the tumors, likely due to the antiangiogenic effects causing tumor cell death and limiting virus spread and production (n = 6). Error bars represent SEM. Bev, bevacizumab; IP, intraperitoneal; ITu, intratumoral; oHSV, oncolytic herpes simplex virus; pfu, plaque-forming unit.

combination therapy may be in part due to enhanced virus production. In contrast to our expectations, oHSV replication was repressed in bevacizumb-treated mice at all time points compared with control mice (**Figure 5c**). oHSV was still detectable at 144 hours post-injection suggesting low-level persistent virus replication. These data show that VEGF blockade inhibits ITu virus production, likely due to antiangiogenic effects leading to tumor cell necrosis, suggesting that enhanced antitumor efficacy of combination therapy is due to factors other than more efficient or widespread virus infection.

Combined therapy with bevacizumab and oHSV enhances antiangiogenesis

Having ruled out enhanced virus replication to account for improved antitumor efficacy, we sought to determine the effect of combination therapy on angiogenesis. Despite a downregulation of tumor-derived VEGF following virus injection, addition of two doses of bevacizumab (3 days apart) further reduced ITu hVEGF by 4.3-fold 6 days after virus injection (**Figure 6a**, $P < 0.05$). Analysis of mVEGF concentrations again showed an increase in oHSV-treated mice, unaffected by bevacizumab (as expected due to its known species specificity; **Figure 6b**). We also detected apoptotic pericytes and endothelial cells in the bevacizumab-treated groups (**Figure 6c,d**), but because such vessels were rare, we were unable to determine whether they were increased in animals treated with combination therapy. Only the combination group showed a statistically significant decrease in vessel numbers though both bevacizumab groups showed a similar decrease in the vessel area per high powered field (microvessel density) (**Figure 6e,f**). Although the differences were mild, the findings of further decreased hVEGF levels and vascularity suggest that enhanced antiangiogenesis may play a role in the improved efficacy of combination therapy.

Enhanced efficacy of combination therapy is unrelated to VEGF levels

To confirm target inhibition by anti-VEGF antibodies, we measured VEGF levels in an *in vitro* assay (data not shown, but the activity of both antibodies on VEGF was confirmed) and determined their effect on virus-induced ITu hVEGF and mVEGF

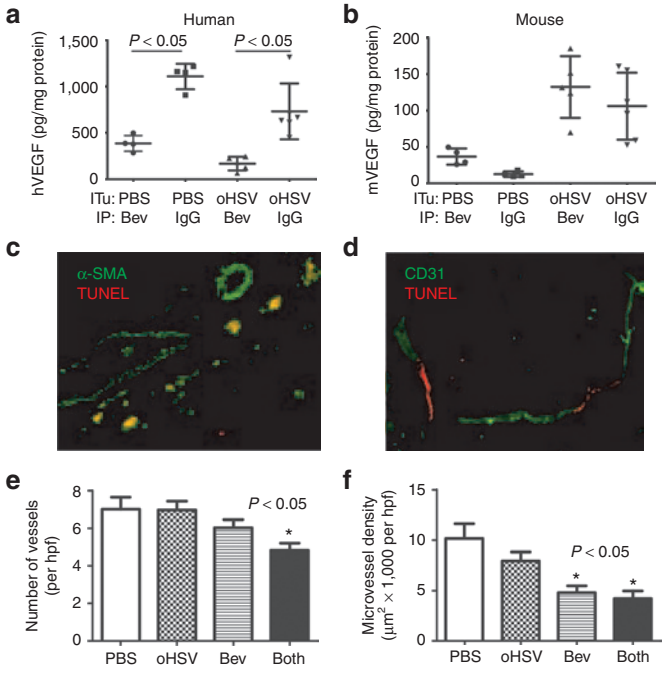

Figure 6 Effects of the combination of intratumoral oHSV and intraperitoneal bevacizumab on the tumor vasculature. A673 tumor-bearing animals were administered either ITu PBS and IP rat IgG control antibody, ITu rRp450 and IP rat IgG control antibody, ITu PBS and IP bevacizumab or ITu rRp450 and IP bevacizumab. Tumors were harvested 3 days post-infection and either analyzed by ELISA for (**a**) hVEGF (n = 4–5) and (**b**) mVEGF (n = 4–6), evaluated by immunohistochemistry for apoptosis by TUNEL staining and for (**c**) pericytes by α-smooth muscle actin (α-SMA) staining or (**d**) endothelial cells by CD31 staining. Error bars represent SD (in **a**,**b**). Tumors were also quantified for (**e**) vessel numbers (n = 6, 10 high power fields per tumor) and (**f**) microvessel density (total vessel area per high power field; n = 6, 10 high power fields per tumor). Error bars represent SEM. Data were compared with PBS and only those indicated by an asterisk reached statistical significance. Bev, bevacizumab; ELISA, enzyme-linked immunosorbent assay; hpf, high power field; hVEGF, human vascular endothelial growth factor; mVEGF, mouse vascular endothelial growth factor; IP, intraperitoneal; ITu, intratumoral; oHSV, oncolytic herpes simplex virus; PBS, phosphate-buffered saline; TUNEL, terminal deoxyribonucleotidyl transferase-mediated dUTP nick end labeling.

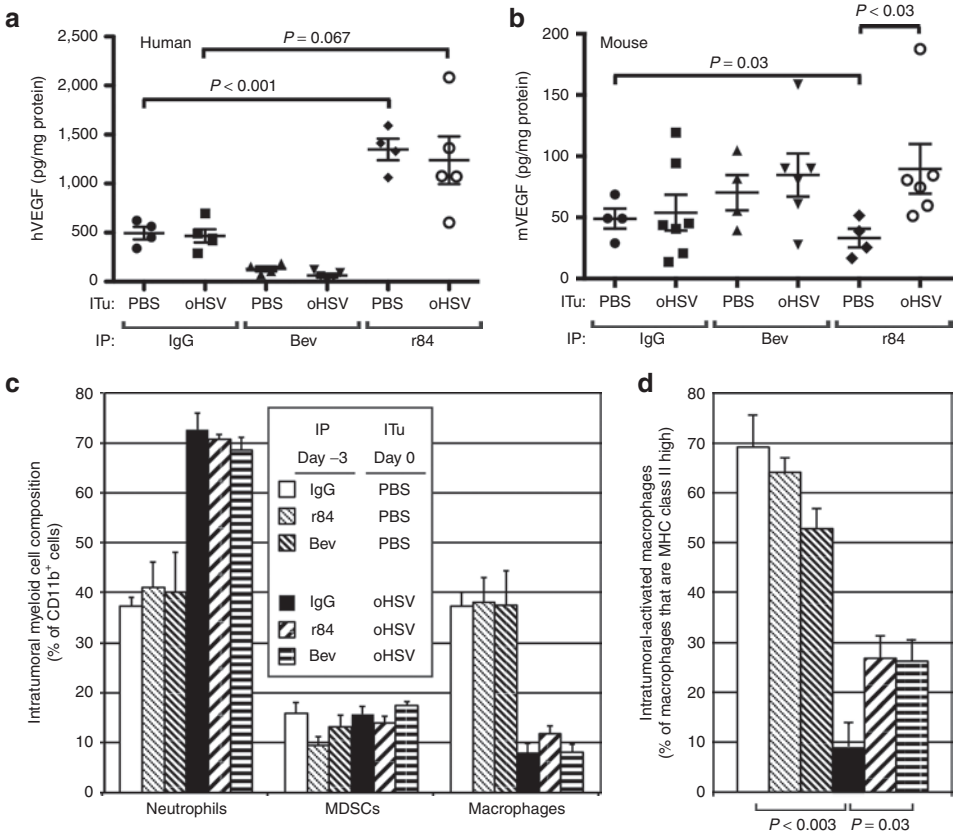

Figure 7 Effect of VEGF blockade on the tumor microenvironment. Tumor-bearing animals were treated with either PBS (control) or oHSV by intratumoral injection and intraperitoneal IgG (control) or anti-VEGF antibodies r84 or bevacizumab. All treatments were given on day 0. Tumors were harvested on day +3 and analyzed for (**a**) tumor-derived hVEGF (n = 4–5), (**b**) host-derived mVEGF (n = 4–7), (**c**) CD11b$^+$ cells by flow cytometry (n = 4) including neutrophils (CD11b$^+$Gr1$^+$F4/80$^-$), myeloid-derived suppressor cells (CD11b$^+$Gr1$^-$F4/80$^-$), and macrophages (CD11b$^+$Gr1$^-$F4/80$^+$), and (**d**) MHC class II-positive macrophages. Error bars represent SEM. Bev, bevacizumab; hVEGF, human vascular endothelial growth factor; mVEGF, mouse vascular endothelial growth factor; IP, intraperitoneal; ITu, intratumoral; MDSC, myeloid-derived suppressor cell; MHC, major histocompatibility complex; oHSV, oncolytic herpes simplex virus; PBS, phosphate-buffered saline.

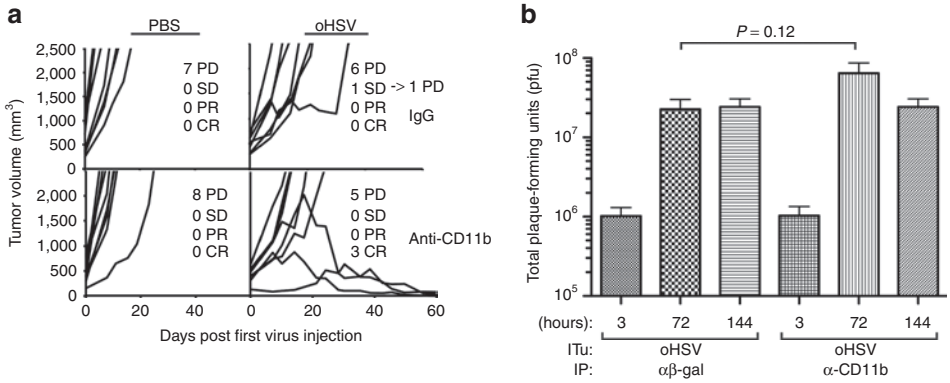

Figure 8 Effect of systemic CD11b$^+$ cell depletion on efficacy of oHSV virotherapy. Sustained antibody-mediated depletion of CD11b$^+$ myeloid cells was achieved before and following intratumoral injection of PBS (control) or oHSV. (**a**) Animals were followed for tumor growth (n = 8). (**b**) In a separate cohort, tumors were harvested at the times shown and analyzed by plaque assay for infectious virus. In contrast to the effects of bevacizumab, which reduced virus replication, depletion of CD11b$^+$ cells had no effect on intratumoral virus production (n = 5–6). Error bars represent SEM. CR, complete response; IP, intraperitoneal; ITu, intratumoral; oHSV, oncolytic herpes simplex virus; PBS, phosphate-buffered saline; PD, progressive disease; pfu, plaque-forming unit; PR, partial response; SD, stable disease.

levels. As expected and consistent with our previous results, bevacizumab decreased baseline and post-virus hVEGF levels and had no effect on mVEGF levels, which were higher following ITu oHSV (Figure 7a,b). Although r84 treatment diminished baseline mVEGF levels, consistent with its known effects on mVEGF, it unexpectedly stimulated baseline hVEGF and post-virus hVEGF and failed to prevent the virus-induced increase in mVEGF levels. Because bevacizumab blocks binding of VEGF to both VEGFR1

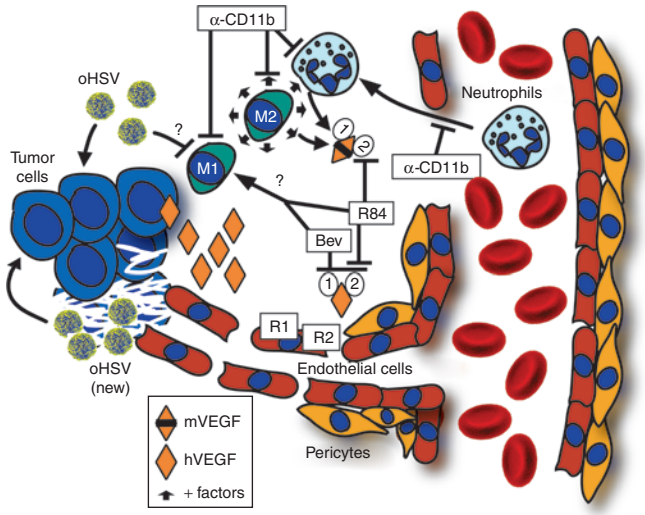

Figure 9 Model of enhancement of oHSV efficacy by VEGF blockade. A model consistent with our data is that virus infection of tumor cells stimulates an innate neutrophilic infiltration and, through an unknown mechanism, depletes M1-type tumor-associated macrophages. Infection also induces production of host-derived mVEGF, either directly or indirectly *via* myeloid cells. The increase in stroma-derived mVEGF is an example of the virus effects on the local tumor microenvironment, but in the A673 model is overshadowed by tumor-derived hVEGF and likely plays only a minor role in angiogenesis. (We postulate that the effect of stroma-derived mVEGF may be more impactful in models with less tumor-derived hVEGF production). The virus-induced $CD11b^+$ infiltrate results in production of protumor growth and proangiogenic factors from neutrophils and M2-type macrophages (+ factors represented by small arrows) that are no longer offset by M1-type macrophages. The combination of oHSV and anti-VEGF is more antiangiogenic, and the resulting tumor cell death is likely responsible for decreased intratumoral virus spread and production. Despite lower virus production, the combination results in improved antitumor effects due in part to modulation of the intratumoral myeloid cell composition, specifically by a mitigation of the decrease in tumoricidal M1-type macrophages. These effects are dependent on VEGFR2 signaling as they were seen with bevacizumab and r84. Modulation of myeloid cells is in part responsible for the combined effects of oHSV with VEGF blockade as it could be recapitulated by combining oHSV with depletion of CD11b cells, possibly by preventing a virus-induced predominance of M2-type compared with M1-type macrophages. The "?" denotes unknown mechanism. Bev, bevacizumab; hVEGF, human vascular endothelial growth factor; mVEGF, mouse vascular endothelial growth factor; oHSV, oncolytic herpes simplex virus; VEGFR, vascular endothelial growth factor receptor.

and VEGFR2, but r84 only blocks binding to VEGFR2, this finding suggests that VEGFR1 signaling in the absence of VEGFR2 signaling results in increased production and/or secretion of VEGF. In addition, these data may explain the more rapid progression of tumors treated with r84 alone (**Supplementary Figure S1e**). In this experiment, we did not clearly see an increase in mVEGF with oHSV alone or in combination with bevacizumab as was shown in **Figure 6b**. We attribute the difference to the tumors being larger in this experiment, which masked the differences between treatment groups, as the outlying higher values with virus were from smaller tumors similar to those used in **Figure 6b**. Regardless, these data clearly show that the enhanced antitumor effect of virotherapy by anti-VEGF antibodies does not correlate with ITu VEGF levels. Given the previously described effects of anti-VEGF antibodies on myeloid cell infiltration,[12] we hypothesized that the enhanced antitumor effect of oHSV with VEGF blockade may be due in part to the modulation of the myeloid stroma microenvironment rather simply an antiangiogenic effect.

r84 and bevacizumab partially mitigate virus-induced depletion of macrophages

We performed a myeloid cellular subset analysis in tumors to further define the effects of virus and anti-VEGF antibodies. In control antibody-treated animals, ITu oHSV induced a marked neutrophilic infiltration ($CD11b^+GR1^+F4/80^-$ cells, **Figure 7c**). Although myeloid-derived suppressor cells ($CD11b^+GR1^+F4/80^+$)[16] were relatively unaffected by virus, the percentage of TAMs ($CD11b^+GR1^-F4/80^+$) dropped significantly following oHSV injection. Further analysis of these cells using major histocompatibility complex (MHC) class II staining revealed a selective depletion of MHC class II expressing TAMs ($CD11b^+GR1$-$F4/80^+$class II^{hi}) by virus (**Figure 7d**), suggesting virus infection alters the balance of ITu macrophages. Although the neutrophilic infiltration was unaffected by pre-treatment with either r84 or bevacizumab, these anti-VEGF antibodies partially prevented the drop in MHC class II expressing macrophages. Given the lack of correlation of VEGF levels with combined oHSV and anti-VEGF efficacy, these data suggest that anti-VEGF antibodies may enable the antitumor effects of virotherapy in part by modulating the ITu composition of myeloid cells.

Myeloid cell depletion enhances oHSV antitumor efficacy

To directly determine whether ITu myeloid cells mitigate the antitumor activity of oHSV, we achieved sustained systemic depletion of $CD11b^+$ cells before and following virus injection. Depletion of $CD11b^+$ cells resulted in an enhanced antitumor effect of virotherapy, with three of eight mice exhibiting a complete response (**Figure 8a**). As before with bevacizumab, the effect did not appear to be due to enhanced virus production as only a small increase in oHSV replication was observed that did not reach statistical significance (**Figure 8b**). These data confirm that the cellular host response to virus infection mitigates antitumor effects of virotherapy. Further, our data strongly suggest the enhancement of virotherapy by anti-VEGF antibodies is due in part to their modulation of virus-induced changes in ITu myeloid cells.

DISCUSSION

We studied a sarcoma model highly susceptible to cytolytic oHSV infection in tissue culture but which lacks significant antitumor response *in vivo*. We found that ITu oHSV injection is associated with an acute inflammatory neutrophilic infiltrate, concomitant decrease of TAMs, and upregulation of host-derived VEGF dependent upon ITu $CD11b^+$ cells. Despite the increased mVEGF following virus infection, total ITu VEGF levels fell after virus injection due to the decreased tumor-derived contribution, yet the antiangiogenic effects of virus alone were mild. VEGF blockade with bevacizumab further decreased angiogenesis and partially mitigated the drop in TAMs, the latter being likely due to interference with VEGFR2 signaling as it was observed with both bevacizumab and r84. Most importantly, the enhanced antitumor effect of oHSV with VEGF blockade was in large part recapitulated by

oHSV combined with systemic depletion of CD11b$^+$ cells, providing strong support for the notion that the ITu myeloid cell response to virus infection modulates the efficacy of virotherapy.

A model consistent with our observations is shown in **Figure 9**. Because M1-type macrophages are tumoricidal whereas M2-type are tumorigenic,[11] a selective decrease of M1-type macrophages by virus infection without affecting the M2-type macrophages might be counterproductive for virus-driven antitumor effects and would explain our findings. Prevention of this imbalance either by anti-VEGF therapy or depletion of CD11b$^+$ cells altogether would then be antitumorigenic.

Our data are partly consistent with previous observations of increased innate inflammatory cell infiltration following injection of oHSV. Prior administration of the antiangiogenic agent cilengitide markedly decreased the overall extent of leukocyte infiltration and improved antitumor efficacy of oHSV in an immunocompetent rat glioma model.[17] Infection of glioma cell lines with the oHSV G207 but not G47Δ decreased thrombospondin-1 and thrombospondin-2 levels without affecting VEGF and matrix metalloproteinase levels, leading to an overall increase in microvascular density.[18] In fact, tissue studies in clinical trials of patients injected with oHSV are consistent with a proangiogenic host response.[19] The neutrophilic infiltration we observed was similar to that seen with oHSV-2 mutant.[20] In contrast to studies of bevacizumab on adenovirus in xenograft models of thyroid carcinoma[21] and on oHSV in a gliomamodel,[22] however, we did not find enhanced virus replication due to bevacizumab. In fact, we found less virus in tumors treated with bevacizumab, likely due to inhibition of virus spread from cell death. Furthermore, prevention of the cellular infiltrate by depletion of CD11b$^+$ cells either had little or no effect on virus production.

Wild-type HSV-1 infection of the mouse cornea results in upregulation of matrix metalloproteinase-9 and VEGF by infiltrating neutrophils.[7,8] We have previously shown that inhibition of matrix metalloproteinase activity by an oHSV-expressing tissue inhibitor of metalloproteinases-3 decreases angiogenesis, recruitment of bone marrow-derived endothelial precursors, and leads to better antitumor efficacy in xenograft tumor models.[23] oHSV armed with various antiangiogenic molecules have shown improved antitumor effects.[22,24–28] Our findings raise the possibility that these viruses engineered to be enhanced for antiangiogenic activity may also be functioning in part by modulating the innate cellular immune response to virus infection.

Whether or not the innate inflammatory response is deleterious to oHSV's antitumor effect appears to depend on the tumor model. Whereas A673 tumors exhibited minimal response to oHSV itself, virotherapy alone was highly effective at shrinking 143.98.2 tumors. The difference was not due to differences in tumor cell autonomous susceptibility to virus infection, which were similar in cultured cells. One testable possibility is that 143.98.2 cells induce a less robust innate host reaction following oHSV infection. It will be interesting to determine in future studies whether the VEGF and cellular inflammatory responses vary among different tumor models.

Although the current studies are limited to the innate host immune response, the adaptive T-cell response also plays an important role in the efficacy of oncolytic virotherapy.[29–32] Further studies will be needed to determine whether modulation of the innate response, as we have done with VEGF blockade, will compromise the downstream adaptive immunity to tumor antigens. Targeted therapy for specific counterproductive aspects of the immune response, while ultimately preserving the adaptive immune response, is likely to be a more effective strategy than global immunosuppression.

In conclusion, we found that systemic VEGF blockade significantly enhances oHSV virotherapy in part due to enhanced antiangiogenesis but also due to modulation of the innate cellular host response. Our results may also explain in part, the improved efficacy, we previously observed using intravenous oHSV and bevacizumab.[33] Because bevacizumab is Food and Drug Administration approved, clinical trials in combination with oHSV virotherapy are thus warranted. Our findings add to the growing literature supporting the notion that understanding and circumventing host-derived barriers may help enable the full antitumor potential of oncolytic virotherapy for cancer.

MATERIALS AND METHODS

Cells and viruses. Human cancer cell lines RD (embryonal RMS), Rh30 (alveolar RMS), 143.98.2 (OS), and A673 (Ewing sarcoma) were all obtained from ATCC (Manassas, VA). Although A673 is catalogued as an RMS, it was derived from a human peripheral neuroepithelioma (25) and the presence of the EWS/FLI1 transcript (26) confirmed it to be a member of the Ewing sarcoma family tumors. The African Green Monkey kidney cell line, Vero, was purchased from ATCC and used in the standard plaque assay. RD and A673 cells were grown in Dulbecco's modified Eagle's medium and 10% fetal bovine serum supplemented with 100 U/ml penicillin, and 100 mg/ml streptomycin. Vero was grown in MEM-E (ATCC) and 10% fetal bovine serum supplemented as above. ICP6-deleted rRp450 HSV-1 (oHSV) was kindly provided by E. Antonio Chiocca (Ohio State University, Columbus, OH).

Animal studies. Animal studies were approved by the Cincinnati Children's Hospital Medical Center Institutional Animal Care and Use Committee. Mice were euthanized per institutional guidelines once tumor size reached 10% of body weight. Six to eight weeks old female athymic nude (nu/nu) mice (Harlan Sprague Dawley, Indianapolis, IN) were injected subcutaneously with A673 Ewing sarcoma cells (5×10^6) in 30% matrigel (BD Biosciences, San Diego, CA). Tumor volume was determined by $V = (L \times W^2) \times \pi/6$, where V is the volume, L is the length of the tumor, and W is the width. When tumor volume exceeded 200 mm^3, mice were randomized to receive treatment. rRp450 virus injections were given ITu at 1.0×10^7 plaque-forming units (pfu)/dose in 100 µl of PBS given in a fractionated fashion as previously described.[34] Control animals were injected similarly with 100 µl PBS. Bevacizumab and r84 antibody or nonspecific rat IgG (control) were given by IP injection at 10 mg/kg. For survival experiments, bevacizumab and r84 were given at 10 mg/kg twice weekly. For tumor vasculature studies, animals bearing A673 tumors ranging from 150–1,000 mm^3 were injected with either PBS (ITu) and the rat IgG control antibody (IP) at 10 mg/kg, rRp450 (ITu) at 1.0×10^7 pfu and the rat IgG control antibody (IP) at 10 mg/kg, PBS (ITu) and bevacizumab (IP) at 10 mg/kg, or rRp450 at 1.0×10^7 pfu and bevacizumab (IP) at 10 mg/kg. ITu virus or PBS were given on days 0 and 2, while antibodies were given twice weekly.

Immunohistochemistry. The spleen and tumor from each mouse in each treatment group were harvested at 24 hours after virus injection, incubated overnight in 30% sucrose and snap-frozen using Tissue-Tek Optimal Cutting Compound (Fisher Scientific, Pittsburgh, PA). Tissues were cut into 5-µ frozen sections and stained with monoclonal rat anti-Ly6g (Clone

1A8, 1:25 dilution) for neutrophil-specific marker or its isotype control IgG2a (both from BioLegend, San Diego, CA) for immunohistochemistry using a Mouse-on-Mouse kit and 3,3′-diaminobenzidine peroxidase substrate according to the manufacturer's protocol (Vector Laboratories, Burlingame, CA). Harris hematoxylin was used for counterstaining. Parallel slides were stained using standard hematoxylin and eosin staining by the Nationwide Children's Hospital Research Institute biopathology core.

In vitro *viral cytotoxicity assay.* A673 cells were seeded in 96-well plates. After 2 hours, rRp450 at MOI 0, 0.1, 0.01, 0.001 or bevacizumab at concentrations 10, 100 μg/ml were added in quadriplicates. Cultures were assessed for cell viability on days indicated by Celltiter 96 (Promega, Madison, WI) according to the manufacturer's instructions.

In vitro *viral replication assays.* Cells were plated in 12-well dishes at 5×10^5 cells per well, adhered at 37 °C for 2 hours, and infected using 5×10^3 (MOI of 0.01) or 5×10^4 (MOI of 0.1) virus in a total volume of 0.1 ml. Plates were gently shaken every 10 minutes for 1 hour. Inoculum was removed after 1 hour and replaced with 0.5 ml fresh media. At times indicated, cells were scraped, freeze-thawed two times, diluted, and titered by standard plaque assay.

In vivo *viral replication assays.* A673 xenograft tumors were established in athymic nude mice by injecting 1.0×10^6–5.0×10^6 cells subcutaneously in the right flank. Tumor growth was measured by the length and width using calipers two times per week. When tumor volume was 250–350 mm^3, animals were randomized to receive IP bevacizumab or IP rat IgG isotype (control) at day −3 and ITu oHSVat day 0. Mice were killed at day +3 and tumors harvested for plaque assays.

$CD11b^+$ myeloid cell depletion with monoclonal antibody. To deplete $CD11b^+$ myeloid cells ($GR1^-F4/80-$), 6–8 weeks old athymic nude mice bearing A673 tumors were administered IP with either 400 μg of anti-β-gal control antibody (clone GL113) or 400 μg of anti-$CD11b^+$ antibody (clone M1/70) on days −2, −1, 0, +1, +2 and ITu with either 100 μl of PBS (control) or 1.0×10^7 pfu rRp450 (oHSV) in 100 μl of PBS on day 0. Tumors were collected at day +3 and analyzed by flow cytometry for cellular infiltrate and by enzyme-linked immunosorbent assay for mVEGF levels. For tumor growth and survival studies, animals bearing A673 tumors ranging from 150–800 mm^3 were administered IP with α-CD11b at days −2, −1, 0, +1, +2, and daily on days +5 through +9 for a total of 10 doses and PBS or rRp450 (oHSV) at day 0 and 7.

Enzyme-linked immunosorbent assay for VEGF production. Harvested tumors were snap-frozen in liquid nitrogen and stored at −80 °C until processed. Tumors were homogenized with a Powergen tissue homogenizer (Fisher Scientific) in 1 ml of a protease cocktail inhibitor (Roche, Indianapolis, IN). The tumor lysates were freeze-thawed twice and centrifuged at 4,000*g* at 4 °C for 10 minutes. The supernatants were assayed for mVEGF and hVEGF using appropriate sandwich ELISA kit (R&D systems, Minneapolis, MN) according to the manufacturer's instructions. Purified recombinant protein provided in the kits was used as positive controls and to create standard curves.

Flow cytometry. Animals bearing A673 tumors >200 mm^3 were administered IP with either rat IgG (control), bevacizumab, or r84 and PBS (control) or rRp450 (oHSV) at day 0. Animals were killed on day 3. Harvested tumors were digested using Liberase Blendzyme 3 (Roche, Mannheim, Germany) and passed through a 100 nm filter to achieve a homogeneous cellular suspension and remove tumor extracellular matrix. After obtaining single cell suspensions, 1×10^6 cells were stained with antibodies against GR-1 (FITC, clone Ly6G, generated in-house), MHC Class II (PerCP, clone 3F12-35, generated in-house), CD11b (clone M1/70; BD Biosciences), CD11c (eFluor450(PB), clone N418; eBioscience, San Diego, CA), and F4/80 (APC, clone BM8; eBioscience) according to standard surface staining protocol. Data was acquired on LSRII flow cytometer and analyzed using FACSDiva software (BD Biosciences).

Protein assay. Supernatants from tumor lysates were diluted 1:20 with double deionized water. Protein was assayed using the bicinchoninic acid method (Pierce, Rockford, IL) according to the manufacturer's instructions.

Immunofluorescence. After harvesting tumors on day 3 post-injection, the tumors were formalin-fixed and paraffin-embedded. Sections were cut at 5 μm and placed on charged glass slides. Tumor tissue slides were heated at 65 °C for 30 minutes, deparaffinized, and rehydrated. Antigen Retrieval Solution (DAKO, Carpinteria, CA), 3% hydrogen peroxide, and Protein Block Solution (DAKO) were sequentially applied to prepare the tissue slides. They were then incubated with Meca-32 primary monoclonal antibody (1:10, Developmental Studies Hybridoma Bank, University of Iowa, Iowa City, IA) for 60 minutes at room temperature. Biotinylated secondary antibody (Vector Laboratories) was applied at 1:200 dilution for 30 minutes and detected using Fluorescein Avidin D (Vector Laboratories). The slides were mounted with Vectashield medium containing DAPI (Vector Laboratories). Terminal deoxyribonucleotidyl transferase-mediated dUTP nick end labeling (TUNEL) staining was performed using the ApopTag Red In Situ Apoptosis Detection Kit (Millipore, Billerica, MA) according to the manufacturer's instructions. Staining with Meca-32 antibody (1:10 dilution) was incorporated into the TUNEL protocol.

Microvessel numbers and density. Tumor tissue slides were analyzed by fluorescence microscopy using the Nikon 90i with NIS-Advanced Elements software (Nikon Instruments, Melville, NY). Ten vascular "hotspots" were identified on each section and used for vessel quantification. Mean vessel numbers within each tumor tissue slide were determined using manual measurements by two blinded independent investigators. Data are expressed as numbers of vessels per 200× field. Vascular area was determined from the individual vascular cross-sectional measurements and quantified using the NIS-Advanced Elements software. Microvessel density was calculated as the ratio of the total microvascular area per 200× field (high power field).

Statistical analysis. Comparisons between two means were performed with an unpaired Student's *t*-test and more than two means by analysis of variance. Survival was analyzed by log-rank. All statistics were done using GraphPad Prism 5 software (GraphPad Software, La Jolla, CA).

SUPPLEMENTARY MATERIAL

Figure S1. *In vivo* efficacy of rRp450 combined with VEGF blockade.

ACKNOWLEDGMENTS

We thank Daniel Demopoulos, Cindy Lambert, Steve Mayer, and Cindy Klotz (Hematology/Oncology pharmacy at Cincinnati Children's Hospital Medical Center) for providing bevacizumab, E. Antonio Chiocca (Ohio State University) for providing rRp450, and Arturo Maldonado (Cincinnati Children's Hospital Medical Center) for help with statistical analyses. This work was supported by Cincinnati Children's Hospital Medical Center, Division of Hematology/Oncology, Nationwide Children's Hospital Research Institute, The Limb Preservation Foundation (F.K.E.), teeoffagainstcancer.org, the Katie Linz Foundation, TeamConnor.org, CancerFree Kids, the American Cancer Society (F.K.E.), and National Institutes of Health grant R01-CA114004 (T.P.C.). R.A.B.'s lab is supported in part by Affitech AS, a company developing r84, and L.B. is employed by Bioceros. The other authors declared no conflict of interest.

REFERENCES

1. Shen, Y and Nemunaitis, J (2006). Herpes simplex virus 1 (HSV-1) for cancer treatment. *Cancer Gene Ther* **13**: 975–992.
2. Hammill, AM, Conner, J and Cripe, TP (2010). Oncolytic virotherapy reaches adolescence. *Pediatr Blood Cancer* **55**: 1253–1263.

3. Wuest, TR and Carr, DJ (2010). VEGF-A expression by HSV-1-infected cells drives corneal lymphangiogenesis. *J Exp Med* **207**: 101–115.
4. Cook, WJ, Kramer, MF, Walker, RM, Burwell, TJ, Holman, HA, Coen, DM *et al.* (2004). Persistent expression of chemokine and chemokine receptor RNAs at primary and latent sites of herpes simplex virus 1 infection. *Virol J* **1**: 5.
5. Fenton, RR, Molesworth-Kenyon, S, Oakes, JE and Lausch, RN (2002). Linkage of IL-6 with neutrophil chemoattractant expression in virus-induced ocular inflammation. *Invest Ophthalmol Vis Sci* **43**: 737–743.
6. Kim, B, Sarangi, PP, Lee, Y, Deshpande Kaistha, S, Lee, S and Rouse, BT (2006). Depletion of MCP-1 increases development of herpetic stromal keratitis by innate immune modulation. *J Leukoc Biol* **80**: 1405–1415.
7. Zheng, M, Deshpande, S, Lee, S, Ferrara, N and Rouse, BT (2001). Contribution of vascular endothelial growth factor in the neovascularization process during the pathogenesis of herpetic stromal keratitis. *J Virol* **75**: 9828–9835.
8. Lee, S, Zheng, M, Kim, B and Rouse, BT (2002). Role of matrix metalloproteinase-9 in angiogenesis caused by ocular infection with herpes simplex virus. *J Clin Invest* **110**: 1105–1111.
9. Solinas, G, Germano, G, Mantovani, A and Allavena, P (2009). Tumor-associated macrophages (TAM) as major players of the cancer-related inflammation. *J Leukoc Biol* **86**: 1065–1073.
10. Mantovani, A and Sica, A (2010). Macrophages, innate immunity and cancer: balance, tolerance, and diversity. *Curr Opin Immunol* **22**: 231–237.
11. Doedens, AL, Stockmann, C, Rubinstein, MP, Liao, D, Zhang, N, DeNardo, DG *et al.* (2010). Macrophage expression of hypoxia-inducible factor-1 alpha suppresses T-cell function and promotes tumor progression. *Cancer Res* **70**: 7465–7475.
12. Roland, CL, Lynn, KD, Toombs, JE, Dineen, SP, Udugamasooriya, DG and Brekken, RA (2009). Cytokine levels correlate with immune cell infiltration after anti-VEGF therapy in preclinical mouse models of breast cancer. *PLoS ONE* **4**: e7669.
13. Roland, CL, Dineen, SP, Lynn, KD, Sullivan, LA, Dellinger, MT, Sadegh, L *et al.* (2009). Inhibition of vascular endothelial growth factor reduces angiogenesis and modulates immune cell infiltration of orthotopic breast cancer xenografts. *Mol Cancer Ther* **8**: 1761–1771.
14. Sullivan, LA, Carbon, JG, Roland, CL, Toombs, JE, Nyquist-Andersen, M, Kavlie, A *et al.* (2010). r84, a novel therapeutic antibody against mouse and human VEGF with potent anti-tumor activity and limited toxicity induction. *PLoS ONE* **5**: e12031.
15. Brekken, RA, Overholser, JP, Stastny, VA, Waltenberger, J, Minna, JD and Thorpe, PE (2000). Selective inhibition of vascular endothelial growth factor (VEGF) receptor 2 (KDR/Flk-1) activity by a monoclonal anti-VEGF antibody blocks tumor growth in mice. *Cancer Res* **60**: 5117–5124.
16. Wongthida, P, Diaz, RM, Galivo, F, Kottke, T, Thompson, J, Melcher, A *et al.* (2011). VSV oncolytic virotherapy in the B16 model depends upon intact MyD88 signaling. *Mol Ther* **19**: 150–158.
17. Kurozumi, K, Hardcastle, J, Thakur, R, Yang, M, Christoforidis, G, Fulci, G *et al.* (2007). Effect of tumor microenvironment modulation on the efficacy of oncolytic virus therapy. *J Natl Cancer Inst* **99**: 1768–1781.
18. Aghi, M, Rabkin, SD and Martuza, RL (2007). Angiogenic response caused by oncolytic herpes simplex virus-induced reduced thrombospondin expression can be prevented by specific viral mutations or by administering a thrombospondin-derived peptide. *Cancer Res* **67**: 440–444.
19. Sahin, TT, Kasuya, H, Nomura, N, Shikano, T, Yamamura, K, Gewen, T *et al.* (2012). Impact of novel oncolytic virus HF10 on cellular components of the tumor microenviroment in patients with recurrent breast cancer. *Cancer Gene Ther* **19**: 229–237.
20. Fu, X, Tao, L, Rivera, A, Xu, H and Zhang, X (2011). Virotherapy induces massive infiltration of neutrophils in a subset of tumors defined by a strong endogenous interferon response activity. *Cancer Gene Ther* **18**: 785–794.
21. Libertini, S, Iacuzzo, I, Perruolo, G, Scala, S, Ieranò, C, Franco, R *et al.* (2008). Bevacizumab increases viral distribution in human anaplastic thyroid carcinoma xenografts and enhances the effects of E1A-defective adenovirus dl922-947. *Clin Cancer Res* **14**: 6505–6514.
22. Zhang, W, Fulci, G, Buhrman, JS, Stemmer-Rachamimov, AO, Chen, JW, Wojtkiewicz, GR *et al.* (2012). Bevacizumab with angiostatin-armed oHSV increases antiangiogenesis and decreases bevacizumab-induced invasion in U87 glioma. *Mol Ther* **20**: 37–45.
23. Mahller, YY, Vaikunth, SS, Ripberger, MC, Baird, WH, Saeki, Y, Cancelas, JA *et al.* (2008). Tissue inhibitor of metalloproteinase-3 via oncolytic herpesvirus inhibits tumor growth and vascular progenitors. *Cancer Res* **68**: 1170–1179.
24. Wong, RJ, Chan, MK, Yu, Z, Ghossein, RA, Ngai, I, Adusumilli, PS *et al.* (2004). Angiogenesis inhibition by an oncolytic herpes virus expressing interleukin 12. *Clin Cancer Res* **10**: 4509–4516.
25. Liu, TC, Zhang, T, Fukuhara, H, Kuroda, T, Todo, T, Canron, X *et al.* (2006). Dominant-negative fibroblast growth factor receptor expression enhances antitumoral potency of oncolytic herpes simplex virus in neural tumors. *Clin Cancer Res* **12**: 6791–6799.
26. Liu, TC, Zhang, T, Fukuhara, H, Kuroda, T, Todo, T, Martuza, RL *et al.* (2006). Oncolytic HSV armed with platelet factor 4, an antiangiogenic agent, shows enhanced efficacy. *Mol Ther* **14**: 789–797.
27. Hardcastle, J, Kurozumi, K, Dmitrieva, N, Sayers, MP, Ahmad, S, Waterman, P *et al.* (2010). Enhanced antitumor efficacy of vasculostatin (Vstat120) expressing oncolytic HSV-1. *Mol Ther* **18**: 285–294.
28. Yoo, JY, Haseley, A, Bratasz, A, Chiocca, EA, Zhang, J, Powell, K *et al.* (2012). Antitumor efficacy of 34.5ENVE: a transcriptionally retargeted and "Vstat120"-expressing oncolytic virus. *Mol Ther* **20**: 287–297.
29. Endo, T, Toda, M, Watanabe, M, Iizuka, Y, Kubota, T, Kitajima, M *et al.* (2002). In situ cancer vaccination with a replication-conditional HSV for the treatment of liver metastasis of colon cancer. *Cancer Gene Ther* **9**: 142–148.
30. Toda, M, Rabkin, SD, Kojima, H and Martuza, RL (1999). Herpes simplex virus as an in situ cancer vaccine for the induction of specific anti-tumor immunity. *Hum Gene Ther* **10**: 385–393.
31. Todo, T, Martuza, RL, Dallman, MJ and Rabkin, SD (2001). In situ expression of soluble B7-1 in the context of oncolytic herpes simplex virus induces potent antitumor immunity. *Cancer Res* **61**: 153–161.
32. Todo, T, Rabkin, SD, Sundaresan, P, Wu, A, Meehan, KR, Herscowitz, HB *et al.* (1999). Systemic antitumor immunity in experimental brain tumor therapy using a multimutated, replication-competent herpes simplex virus. *Hum Gene Ther* **10**: 2741–2755.
33. Eshun, FK, Currier, MA, Gillespie, RA, Fitzpatrick, JL, Baird, WH and Cripe, TP (2010). VEGF blockade decreases the tumor uptake of systemic oncolytic herpes virus but enhances therapeutic efficacy when given after virotherapy. *Gene Ther* **17**: 922–929.
34. Currier, MA, Adams, LC, Mahller, YY and Cripe, TP (2005). Widespread intratumoral virus distribution with fractionated injection enables local control of large human rhabdomyosarcoma xenografts by oncolytic herpes simplex viruses. *Cancer Gene Ther* **12**: 407–416.